

X-Ray Spectrophotometer SphinX and Particle Spectrometer STEP-F of the Satellite Experiment CORONAS-PHOTON. Preliminary Results of the Joint Data Analysis

O. V. Dudnik^a, P. Podgorski^b, J. Sylwester^b, S. Gburek^b, M. Kowalinski^b,
M. Siarkowski^b, S. Plocieniak^b, and J. Bakala^b

^a *Kharkiv National University named after V.N. Karazin, Ukraine*

^b *Space Research Center, Polish Academy of Sciences, Solar Physics Division, Wroclaw, Poland*

Received July 18, 2011

Abstract—A joint analysis is carried out of data obtained with the help of the solar X-ray SphinX spectrophotometer and the electron and proton satellite telescope STEP-F in May 2009 in the course of the scientific space experiment CORONAS-PHOTON. In order to determine the energies and particle types, in the analysis of spectrophotometer records data are used on the intensities of electrons, protons, and secondary γ -radiation, obtained by the STEP-F telescope, which was located in close proximity to the SphinX spectrophotometer. The identical reaction of both instruments is noted at the intersection of regions of the Brazilian magnetic anomaly and the Earth's radiation belts. It is shown that large area photodiodes, serving as sensors of the X-ray spectrometer, reliably record electron fluxes of low and intermediate energies, as well as fluxes of the secondary gamma radiation from construction materials of detector modules, the TESIS instrument complex, and the spacecraft itself. The dynamics of electron fluxes, recorded by the SphinX spectrophotometer in the vicinity of a weak geomagnetic storm, supplements the information about the processes of radial diffusion of electrons, which was studied using the STEP-F telescope.

DOI: 10.1134/S0038094612020025

INTRODUCTION

The scientific instruments on board the spacecraft, which were specifically designed to study various phenomena and objects, can be based on similar or related sensor structures. Such sensors can respond not only to the targeted type of radiation, but also to other, unexpected types that can be a hindrance to the chosen area of research. Thus, the ABC apparatus, designed to study the characteristics of the fluxes of hard X rays and gamma rays from solar flares and installed aboard the low-orbiting spacecraft CORONAS-F (Glyanenko et al., 2009), accumulated a large amount of information about changing count rates in low-energy and high-energy γ -bands of extrasolar origin. The distribution of count rates, in geographic coordinates of the Earth, clearly showed the area of the polar caps, radiation belts (RBs), and the Brazilian Magnetic Anomaly (BMA) (Arkhangelskaja et al., 2008). With this apparatus, burst events and quasi-stationary equatorial eruptions of different types were also observed.

The X-ray SphinX spectrophotometer was designed and manufactured at the Solar Physics Division of the Space Research Center of the Polish Academy of Sciences as a part of the Foton scientific equipment of the CORONAS-PHOTON spacecraft (Kotov, 2011). It was designed to study the spectra of solar

X-rays in the energy range 1.2–15 keV. The primary data processing showed that the count rates of sensor units in high energy channels are different from zero even during spacecraft nights. The count rate increased sharply with the passage of regions of the BMA and RBs by the satellite, suggesting a possible recording of high energy particles by the spectrophotometer.

The sensor unit STEP-FD of the electron and proton satellite telescope STEP-F, whose main objective was to study the dynamics of fluxes of high-energy charged particles, was located in close proximity to the SphinX spectrophotometer. Thus, there was an opportunity to conduct a joint analysis of data from the particle detection channels of the SphinX spectrophotometer and STEP-F telescope channels for recording electrons, protons, and secondary gamma radiation. The analysis of data with a 30-second time resolution was performed for the observation period from May 1 to May 14, 2009.

X-RAY SphinX SPECTROPHOTOMETER AND SATELLITE TELESCOPE FOR ENERGETIC PARTICLES STEP-F

Four silicon PIN photodiodes served as solar X-ray sensors of the SphinX spectrometer (Sylwester et al., 2008; Gburek et al., 2011a; 2011b). These detectors

Table 1. The names and characteristics of the recording channels and the respective detectors of SphinX and STEP-F devices

Detector/channel name	SphinX		STEP-F			
	Det1	Det2	D1e	D1p	D2e	D4e
Recorded energy range, MeV	—	—	electrons $\Delta E_e = 0.18\text{--}0.51$ + protons $\Delta E_p = 3.5\text{--}3.7$	protons $\Delta E_p = 3.7\text{--}7.4$ + electrons $\Delta E_e = 0.55\text{--}0.95$	electrons $\Delta E_e = 0.35\text{--}0.95$	Secondary γ -radiation from electrons with $E_e \geq 0.6\text{--}0.8$
Detector type	Si PIN	Si PIN	Si PIN	Si PIN	Si PIN	CsI(Tl) + vacuum photomultiplier
Detector thickness, μm	500	500	380	380	380	5000
Active area, cm^2	0.215*	0.111*	17	17	17	49

* The active area of the detector for particle detection is limited by the internal collimator. In order to register X-rays, the active area has a different value due to the presence of an external collimator (Gburek et al., 2011b).

were independent of each other in information processing. Each sensor is 500 μm thick but with a different active area. Photodiodes were integrated into the sensor units of the XR-100CR type, manufactured by Amptek (<http://www.amptek.com/xr100cr.html>). Against the direct ultraviolet radiation from the Sun, active areas of the detectors were protected by 12.5 μm beryllium foils and 320 nm aluminized Mylar layers. In addition, the sensor with the active area of $S_2 = 0.111 \text{ cm}^2$, indicated further as Det2, was covered by a double plate made of tantalum with a total thickness of 400 μm while maintaining an open detector window of $S_{20} = 4.9 \times 10^{-3} \text{ cm}^2$ for recording X-ray bursts from powerful solar flares. The energy resolution of the apparatus was about 0.4 keV over the entire range of recording $\Delta E = 0\text{--}15 \text{ keV}$, using 256 channels of spectrometric analog-to-digital converters. The minimum energy threshold for signal detection coming from the sensor with the active area of $S_1 = 0.215 \text{ cm}^2$, indicated further as Det1, was set at 1.2 keV. The same characteristic of the detector Det2 was 0.85 keV. Operating reverse-bias voltages for the sensors Det1 and Det2 were set at 130 and 100 V, respectively. The axis of the angle view of the instrument was directed along the axis OZ of the spacecraft, stabilized during the experiment in the direction of the Sun. Angular fields of view of Det1 and Det2 detectors were $1.94^\circ \times 1.94^\circ$ and $1.72^\circ \times 1.72^\circ$, respectively. The time resolution of data recording used in this study was 1 or 5 s, depending on the level of solar activity. In the present analysis, data from the 254 and 255 energy channels of Det1 and Det2 detectors were used.

The electron and proton satellite telescope STEP-F included the STEP-FD sensor unit, mounted on the

platform on the outer surface of the spacecraft, and the digital information processing unit STEP-FE, located with other electronics blocks inside the hermetic chamber filled with an argon-air mixture under a pressure of 1 atm (Dudnik et al., 2011). The detector head of the sensor unit STEP-FD, constructed on the principle of the telescopic system, contained two identical silicon position-sensitive matrix detectors D1 and D2 and two scintillation detectors based on single crystals of CsI(Tl), viewed by silicon photodiodes of a large area in the D3 detection layer and the photomultiplier in the D4 detector. The latter detector, taking into account thicknesses of sensors D3 (13 mm CsI(Tl) + 2 mm MgO) and detectors D1 and D2 (the total thickness of 760 μm), as well as structural materials of aluminum, recorded the secondary gamma photons of low and intermediate energies from the interaction of primary electrons with three layers of detectors and their holders. The total angle of view of the telescope was $108^\circ \times 108^\circ$ for low-energy particles and $98^\circ \times 98^\circ$ for high energy particles. Effective areas of each of the semiconductor detectors were $S_1 = S_2 = 17 \text{ cm}^2$, and of scintillation crystal detectors they were $S_3 = 36$ and $S_4 = 49 \text{ cm}^2$, respectively. Data frames transmitted from the device into the vehicle's system for collecting and recording scientific information every 30 seconds included the average 30-second and 2-second data on types, fluxes, and angular distributions of particles. Table 1 shows some characteristics of the detectors and the energy ranges of devices STEP-F and SphinX used in further analysis.

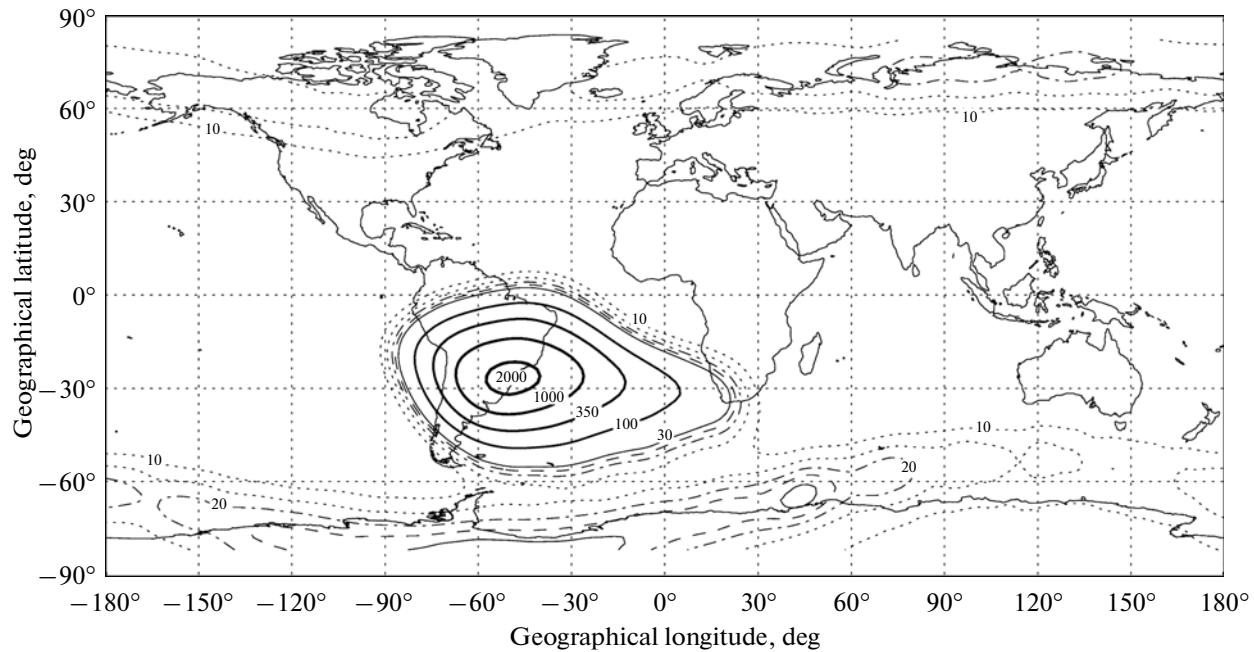


Fig. 1. The count rate distribution in geographic coordinates obtained by the X-ray detector with an active area of 0.111 cm^2 of the SphinX device for the ascending nodes of the spacecraft orbit over the whole observation period from February 20 to November 29, 2009.

THE DISTRIBUTION OF SIGNAL COUNT RATES FROM SphinX SENSORS BY GEOGRAPHICAL COORDINATES

The amplitudes of the signals from SphinX detectors were recorded in 256 channels, corresponding to different X-ray energies, the latter of which were identified as the most sensitive for recording signals from the passage of high-energy particles. Data on the count rates from these last energy channels of the Det1 and Det2 detectors, accumulated over the entire period of observation in 2009, were projected onto a map of the Earth's surface. Fig. 1 shows the distribution of count rates by geographic coordinates recorded by the Det2 detector for the ascending nodes of the satellite orbit.

One can clearly see the areas of the BMA (also known as the South Atlantic Anomaly, SAA) and RBs in the northern and southern hemispheres, characteristic of the distribution of high energy particles. However, the correspondence of records with certain classes and energy ranges of charged particles is unknown due to a lack of prelaunch calibration measurements with charged particles and gamma photons of energies higher than energies of the X-ray range.

The upper part of Fig. 2 shows the distribution of ratios of pulses n_{Det1} , recorded by the Det1 detector to the number of pulses n_{Det2} , recorded by the Det2 detector every 30 seconds over the period from May 1 to 15. Bearing in mind that Det1 and Det2 detectors have different active areas, the numbers of pulses n_{Det1} and n_{Det2} are normalized per unit area.

One can clearly see two maxima, designated by zones 1 and 2, i.e., in zone 1 the ratio $n_{\text{Det1}}/n_{\text{Det2}}$ varies from 0.7 to 1.5, while in the area 2, this ratio varies from 7 to 30 with a broad maximum in the neighborhood of 10–18. The distribution of the number of events corresponding to these two areas by geographical coordinates as obtained for the ascending nodes of the orbit (lower part of Fig. 2) coincides with the contours of the BMA (zone 1) and an outer RB (zone 2). The presence of discontinuities in the data coverage of certain geographical areas is due to limited number of orbital crossings over the period of 14 days. Various $n_{\text{Det1}}/n_{\text{Det2}}$ ratios in different geographical areas represent substantial change in the average energy and character of the particles populating regions of BMA and outer RBs. As a result of differences in the internal construction of Det1 and Det2 detectors, in particular related to presence of additional tantalum protection within Det2. Their energy responses are substantially different. Thus, at each time, and, accordingly, at each point the ratio $n_{\text{Det1}}/n_{\text{Det2}}$ characterizes the slope of the energy spectrum of particles of a given species. A change in the value of $n_{\text{Det1}}/n_{\text{Det2}} \sim 1$ (zone 1) to ~ 15 (zone 2) indicates for a significant difference in the energy spectra of particles populating the BMA and an outer RB.

Another feature of the distribution of $n_{\text{Det1}}/n_{\text{Det2}}$ ratios by geographic coordinates (Fig. 2b) is the north-south asymmetry of the location of points in zone 2. In the southern hemisphere, these points are almost

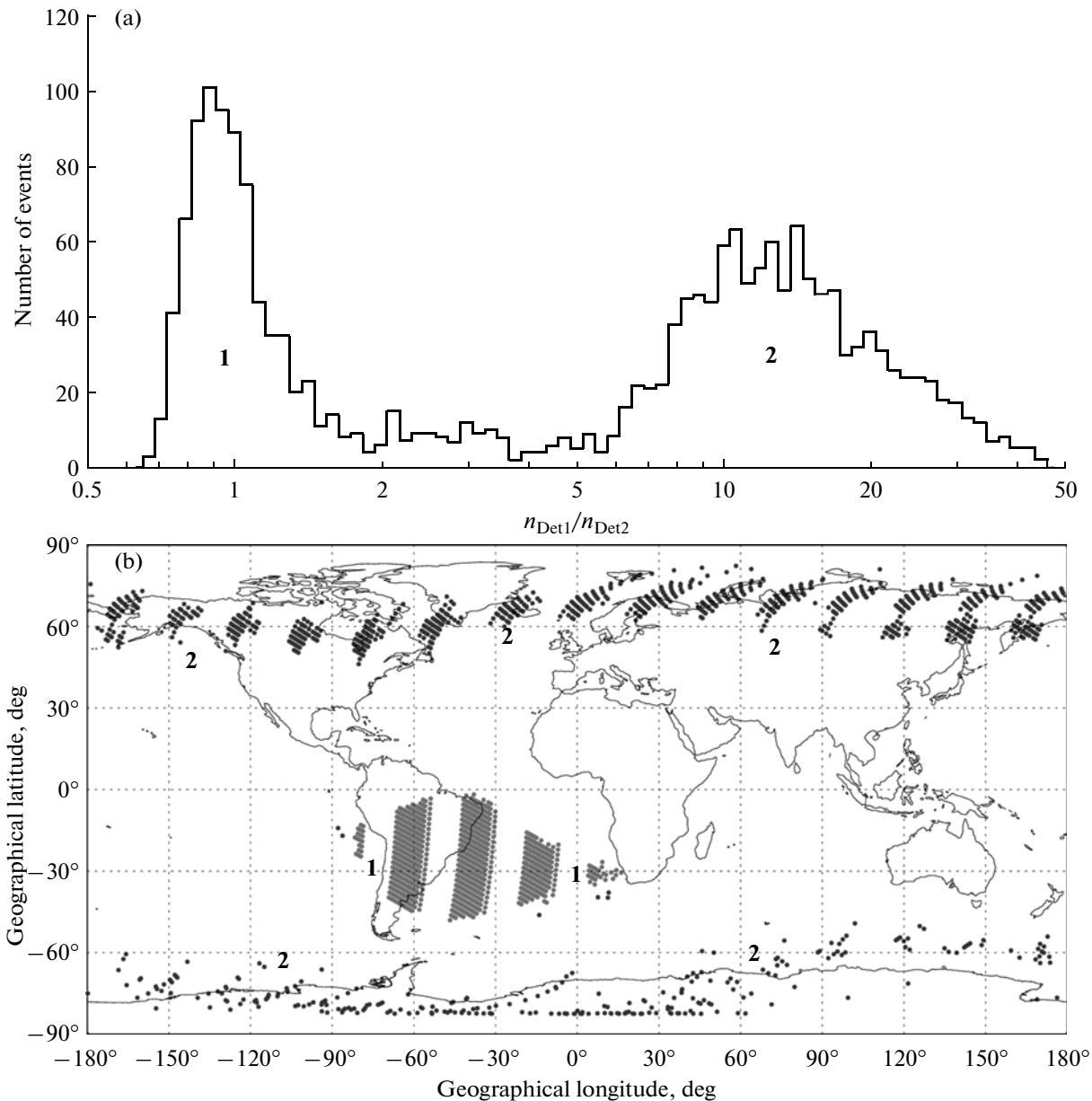


Fig. 2. The distribution of quantities of relations of numbers of pulses n_{Det1} , recorded by the detector Det1 to the number of pulses n_{Det2} , recorded by the detector Det2 from May 1 to 14 (a), and the geographical location of the zones 1 (gray dots indicate the BMA area) and 2 (black points indicate the RB areas) (b).

absent, indicating the measurements being taken at levels very close to background, while in the northern hemisphere values of n_{Det1} and n_{Det2} significantly exceed background readings in the last channels of the spectrometers.

EXPERIMENTAL RESULTS AND ANALYSIS

The analysis of data was performed by comparing the time series of particle fluxes as observed during the geomagnetically quiet time and in the vicinity of a weak magnetic storm with a maximum on May 8,

2009. In addition, the study of dynamical variability of maximum fluxes seen during passages of BMA and RBs regions has been made covering first half of May 2009.

The General View of the Variations of Particle Fluxes, Seen by the Two Instruments

In order to find the best match between energy channels recording electrons and protons by the STEP-F unit, and the respective indications from Det1 and Det2 of the SphinX instrument, the peak of

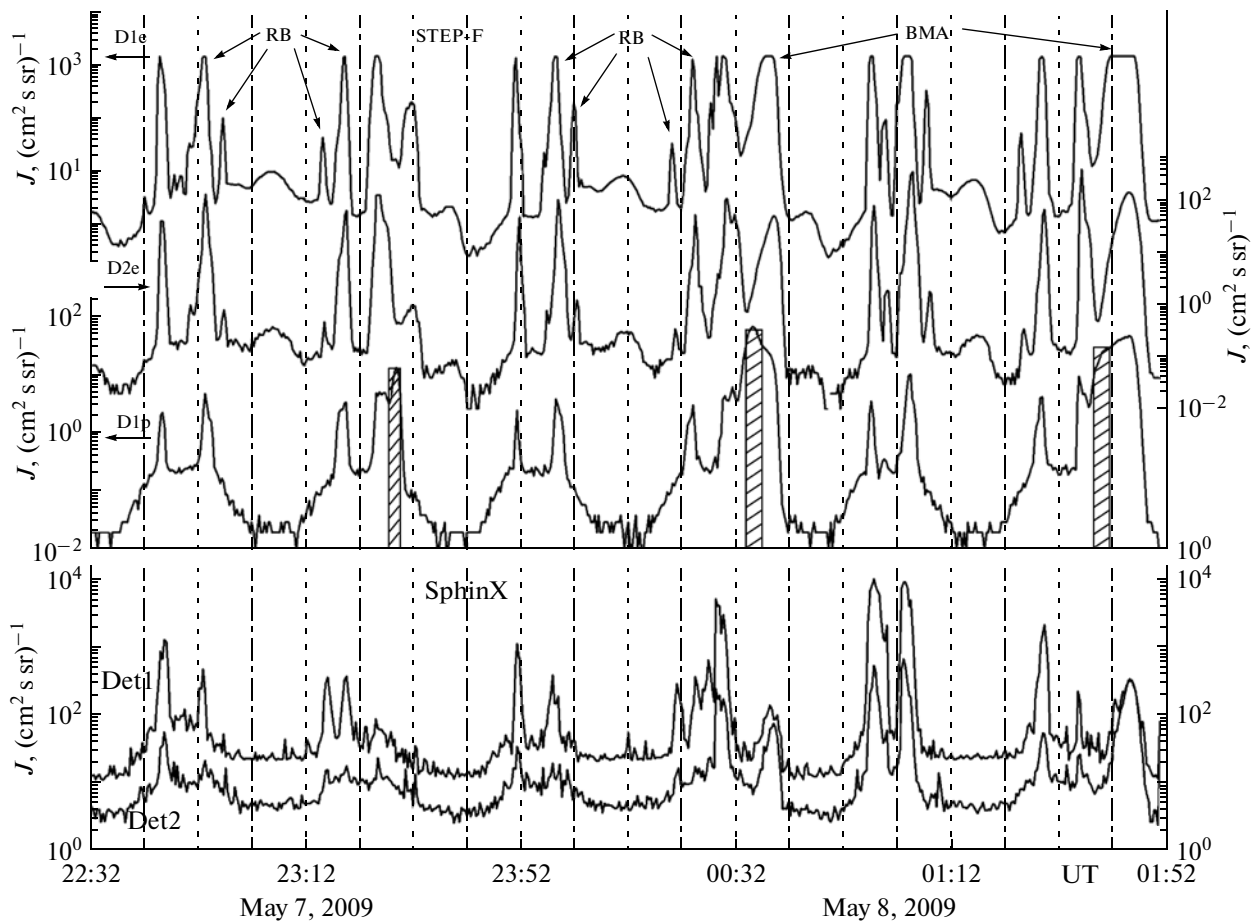


Fig. 3. The time variation of the spectral flux density of high-energy particles recorded by STEP-F and SphinX devices in the period of maximum weak magnetic storm on May 7–8, 2009. UT-universal time, horizontal arrows indicate the ratio of the graphs to the left or right axis OY . The dashed areas indicate periods of recording of low-energy protons in the channel D1p.

the weak geomagnetic storm ($D_{st} = -30$ nT) on May 8 was analyzed. The upper panel of Fig. 3 shows the time variation of the spectral density of the flux of electrons and protons in three energy channels covering few satellite orbits in the period 7–8 May, in comparison with the intensity of particle flow according to the SphinX instrument.

Clearly seen are bumps on the Det1 and Det2 records due to passages of the spacecraft (SC) through RBs and BMA. The SphinX signal enhancement coincides with the increase of electron fluxes in the channels of the STEP-F instrument. Count rates of the Det1 sensor are almost always higher than count rates of Det2 detector by ~ 5 – 10 times. The exception is the area of the BMA, where the count rate measured by both sensors is similar. At the BMA center the count rate in the Det2 becomes even greater than that in the Det1 channel. The latter indicates the sensitivity of the sensor readings to a change in the spectrum of primary particles in different areas of the inner magnetosphere. Sufficiently high count rates of both detectors in very narrow fields of view of $1.94^\circ \times 1.94^\circ$ and $1.72^\circ \times 1.72^\circ$

and the disparity between their relationship and the difference of active areas indicate for presence of the additional component of the channel loading, coming from a larger solid angle. The bremsstrahlung of primary electrons coming from the detector head construction materials, TESIS apparatus, and the spacecraft itself, can serve as such a component, effectively recorded by active layers of the silicon PIN photodiode with a thickness of $500 \mu\text{m}$, operating at reverse-bias voltages of 130 and 100 V, respectively, for Det1 and Det2.

The match between SphinX and STEP-F recordings was not found in the dashed areas in the upper part of Fig. 3, indicating the presence of a substantial response of the D1p channel of the STEP-F device to low-energy protons, and the channels of the SphinX spectrophotometer, which is an additional argument in favor of postulating a positive response of Det1 and Det2 to presence of mixed component of the low-energy electrons and the secondary γ -radiation from electrons at higher energies. The latter circumstance allows us to invoke the concept of effective threshold

energy for detecting electrons E_{thr1} and E_{thr2} by detectors Det1 and Det2, respectively. The actual position of these thresholds can vary depending on the shape of the energy spectrum of primary electrons. The preliminary analysis of the observed modulation in time series studied indicates that the values of E_{thr1} and E_{thr2} are placed in the range of a few hundred keV, but no more than 0.5 MeV. More accurate values of these threshold energies can be obtained by individual comparison of profiles of flux distributions through L-shells (McIlwain L-parameter) within the BMA and in the areas of RB intersection.

A characteristic feature of the response of the SphinX device on the intersection of RBs is a big difference in count rates at the intersection of RBs in the same hemisphere, while the time interval between the intersections is less than 15 minutes.

The Distribution of Maxima of Particle Intensities by L-shells in the BMA

It is known that the values of L-shells at which intensities of the electrons, trapped in radiation belts, take maximum values are different for different particle energies. At the flight altitude of the CORONAS-PHOTON spacecraft orbit, trapped electrons were detected within the BMA. In order to analyze the distributions of particle fluxes through the L-shells, when crossing of the BMA regions took place the fifth since the beginning of the day, turns of ascending nodes of the spacecraft orbit were selected for the comparison. Figure 4 shows an example of the distribution of particle flux densities for four channels of the STEP-F instrument and the two channels the SphinX spectrophotometer as recorded on May 11.

One can see good agreement between the profiles of particle intensities that are displayed in channels D2e, Det1, and Det2. The decrease of the signals when passing from the values of $L \sim 1.25$ to $L \sim 1.85$ is clearly noticeable. Obviously, the Det2 detector is more sensitive to an increase of electron fluxes with higher energies within the BMA. A significant decrease in count rates in this channel at high L-shells indicates a change in the nature of the energy spectrum of primary electrons toward the stronger predominance of particles at low energies. The shape of D1e channel profile between L-shells change from $L \sim 1.5$ to $L \sim 1.9$, a sharp decrease of electron fluxes in D2e and D1p channels in these limits of the McIlwain parameter, and the disappearance of downloads in the D4e channel responsible for the recording of secondary gamma radiation, confirms the change in the character of the energy spectrum of primary electrons.

Table 2 shows the values of L-shells, at which maxima of intensities of particles were recorded between May 1 and May 14, 2009, for five channels of both

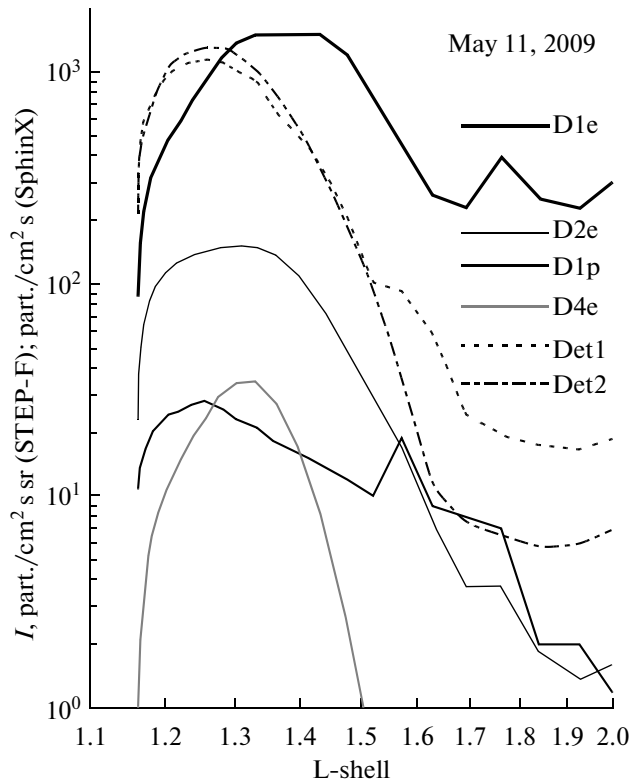


Fig. 4. The intensity distribution of the particles through L-shells within the BMA on the fifth turn since the beginning of the day of the ascending orbit node of the spacecraft on May 11, 2009. Particle fluxes for the SphinX device are not normalized for differences in so-called the solid angle.

devices. For small values of B/B_0 in the BMA, the particle fluxes are close to isotropic and so similar response of SphinX and STEP detectors is observed despite their different fields of view.

L-shell values, averaged for 14 days, allow us to determine the values of E_{thr1} and E_{thr2} for Det1 and Det2 detectors, as well as the effective recording energy for the E_{D4e} detector of the STEP-F device. At the time of the measurements, relationships of the Earth's magnetic field to the magnetic field at the geomagnetic equator for the period considered took values of $B/B_0 \approx 1.2-1.6$.

Figure 5 shows a dependence diagram of L-shell positions, at which maximum particle fluxes were observed, on the energy of the electrons bound to the channels D2e and D1p of the STEP-F device.

The graph shows that the values of E_{thr1} and E_{thr2} are very close to each other, and are ~ 500 keV for Det1 and ~ 475 keV for Det2. However, the scatter of these values is large and is associated not only with a low statistics as recorder for period of 14 days only, but also with the daily displacement of the spacecraft longitudinally at fixed latitude relative to the initial point of measurement, and therefore the observed spectrum of

Table 2. The values of L-shells, on which maximal values of particle fluxes were observed in the period from May 1 to 14, 2009

Day	STEP-F			SphinX	
	D2e	D1p	D4e	Det1	Det2
1	1.35	1.253	1.322	1.296	1.296
2	1.337	1.244	1.337	–	–
3	1.353	1.254	1.324	1.275	1.275
4	1.343	1.247	1.343	1.267	1.29
5	1.333	1.241	1.333	1.282	1.282
6	1.318	1.249	1.318	1.269	1.292
7	1.337	1.242	1.309	1.262	1.284
8	1.3	1.255	1.328	1.276	1.276
9	1.319	1.248	1.319	1.25	1.269
10	1.31	1.242	1.31	1.262	1.262
11	1.302	1.255	1.33	1.255	1.277
12	1.29	1.245	1.316	1.245	1.245
13	1.257	1.237	1.305	1.237	1.257
14	1.27	1.229	1.294	1.248	1.229
Average value	1.315 ± 0.029	1.246 ± 0.007	1.3206 ± 0.013	1.263 ± 0.017	1.272 ± 0.019

electrons transforms from day to day. Accordingly, values of E_{thr1} and E_{thr2} change. Thus, if on May 1 $E_{\text{thr1}} = E_{\text{thr2}} \approx 460$ keV, then for May 12 $E_{\text{thr1}} = E_{\text{thr2}} \approx 550$ keV. From the same graph, the value of E_{D4e} can be determined, which turned out to be $E_{\text{D4e}} \approx 335$ keV. However, the value of E_{D4e} also changed from day to day and varied from 230 to 350 keV in the period between 1 and 14 May. Lower values of the energy of the electron detection by the last detector in the telescope system of the STEP-FD detector block, in comparison with E_{thr1} and E_{thr2} of the SphinX spectrophotometer, are caused by the high efficiency recording of the scintillation detector, its large active area, and very low-noise photomultiplier.

Features of Particle Distributions in RBs

In the Earth's radiation belts fluxes of particles at the altitude of the CORONAS-PHOTON spacecraft are considerably less than in the BMA, therefore there

was an opportunity to use the D1e channel of the STEP-F device in the analysis. This channel had restrictions on the recording at high count rates. The comparison of intensity distributions in recording channels of both units outside the BMA showed the discrepancy of rates of occurrences of the maxima of the count rates in RBs both by time and by the L-shells practically throughout the entire period. The exception was on the days of the maximum and the low initial recovery phase of the geomagnetic storm on May 8–10, when relative distributions of L-shells in the external RBs were very similar. Figure 6 shows the intensity distributions of the particles in recording channels of both instruments in the Northern Hemisphere on May 8 (Fig. 6a) and changes in these distributions in Det1 and Det2 channels of the SphinX unit in the Southern Hemisphere on May 3 and 9 (Fig. 6b).

Fig. 6a shows that the STEP-F device recorded three electron belts in two energy channels, and electrons of the third additional belt (Dudnik, 2010) had a soft energy spectrum, since their intensity drops sharply at $E > 0.55$ MeV. The SphinX spectrophotometer, can also record inner RBs, as evidenced by the steepening of the intensity at $L = 1.6$ and its decline at $2.5 < L < 2.8$ in the Det1 channel, but the sensitivity of the instrument is enough to detect RBs. The second reason, why inner RBs can't be seen explicitly, may consist in the difference between the viewing angles of the two devices. The agreement of distributions by L-shells indicates the appearance of precipitating fluxes with a wide distribution by pitch angle.

To test this hypothesis, the intensity distribution by L-shells in the Southern Hemisphere was built in the two channels for the SphinX spectrophotometer for May 3 and May 9. Figure 6b shows that the device detects the inner RB by the Det1 sensor both in the magnetically quiet period and in the initial recovery phase from the magnetic storm. It also can be seen that the count rate in the Det2 channel, and the sensitivity to changes in fluxes, are significantly lower than in the Det1 channel, which once again confirms the conclusion that channel records higher energy component in the electron spectrum. Thus, the SphinX spectrophotometer with a narrower angle of view compared to the STEP-F device records streams of electrons of both outer and inner RBs, tracking the flux dynamics by both the intensity and radial distributions with regard to the Earth's surface.

THE RADIAL DIFFUSION OF ELECTRONS OF INTERMEDIATE ENERGIES IN THE OUTER RB

The energy spectrum of electrons in the RB is significantly softer than the spectrum in the BMA. In this case, values of E_{thr1} , E_{thr2} , and E_{D4e} for the outer RB

must be different than in the BMA. In order to determine the effective electron energies, two approaches can be applied. The first of them consists in plotting the dependence of averaged values of L-shells, on them maximal values of particle fluxes in the outer RB were observed, against their energy. It is known that the higher the energy of trapped particles, the deeper the layers of the magnetosphere they drift on their way from one magnetic pole to another. Having determined the values of L-shells by Det1 and Det2 detectors of the SphinX spectrophotometer and the D4 detector of the STEP-F telescope, and using the known dependence of the L-shells with particles of maximal intensities from channels D1e, D2e, and D1p of the STEP-F device, we can estimate the values of E_{thr1} , E_{thr2} , and E_{D4e} .

The second approach consists in the determination of the dependence of the displacement ΔL of L-shells, on which maximal values of electron fluxes were observed in geomagnetically quiet days before the start of a magnetic storm and in the recovery phase. The displacement is due to the radial diffusion of electrons in the Earth's magnetic field during the peak of the development and the initial recovery phase of the storm. Numerous satellite experiments show that the magnitude of the displacement ΔL is inversely proportional to the energy of primary electrons (Kuznetsov et al., 2007). Having determined ΔL from data of Det1, Det2, and D4 sensors, and compared it with similar results in channels of the STEP-F device, the values of E_{thr1} , E_{thr2} , and E_{D4e} can be estimated by an independent method.

Figure 7 shows the combined results of the analysis of data obtained for nine days since the beginning of day of ascending nodes of the orbit of the spacecraft in the Northern Hemisphere. Significant variations in values of L-shells (left scale of the OY axis) is due to the presence of a weak magnetic storm in this period, and as a consequence, a displacement ΔL to the region of smaller values of L due to radial diffusion of electrons across the magnetic field lines. The statistical error of values of ΔL (the right scale on the axis OY) cannot be determined because the analysis involved data only from one of the magnetic storm. As a consequence, the graph has a negative value $(\Delta L)_6 = -0.01$. Obviously, the values of ΔL , for which $\Delta L \geq 0.03$ holds true, are applicable to the analysis.

As a result, the analysis of the two graphs in Fig. 7 gives the following values $E_{thr1} \approx 1-5$ keV, $E_{thr2} \approx 60$ keV, and $E_{D4e} \approx 240$ keV. As mentioned above, the Det2 detector was additionally covered by the bilayer tantalum plate with a total thickness of 400 μm while maintaining an open detector window with the area of $4.9 \times 10^{-3} \text{ cm}^2$. With such a thickness of the protective layer of material with a density of $\rho = 16.65 \text{ g/cm}^3$, and charge $Z = 73$, electrons with energies $E_e \geq 1.2 \text{ MeV}$

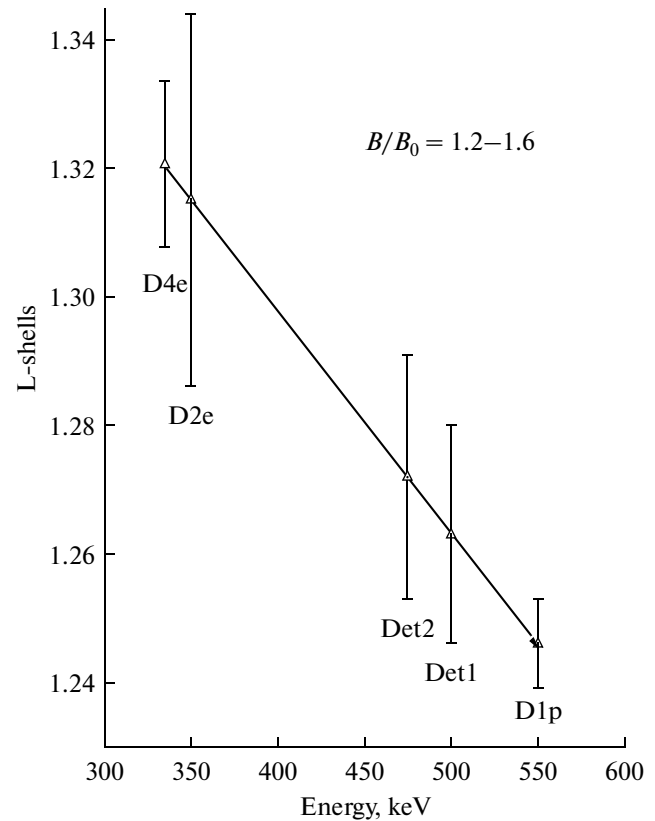


Fig. 5. The dependence of values of L-shells at the maximum of particle fluxes seen in the BMA on energy as determined for ascending nodes of the fifth orbits of the day from May 1 to May 14 2009.

should reach the active volume of the detectors. However, the protective layer itself is a good target for the generation of the secondary gamma radiation of low energies when it is irradiated with high energy primary electrons. The fact that the value of E_{thr2} for the external RB is 10 times less than for the BMA indicates soft spectrum of the RB. The value of E_{thr2} is also reduced by a part of the flux of low-energy electrons entering through the detector window area of $4.9 \times 10^{-3} \text{ cm}^2$ and recorded by the direct method by the active volume of the photodiode. The contribution of direct detection electrons in the total load of the Det1 detector is much higher, but the presence of very low-energy gamma photons cannot be excluded on the basis of the significant count rates for the narrow field of view.

The values of E_{D4e} for the BMA and RBs do not differ greatly from each other due to the selection logic of events in the channel D4e, i.e., the record in this channel is conducted only when the desired signals were simultaneously in all four layers of the detectors of the telescope system of the STEP-FD unit. It means that the electrons producing secondary gamma photons in the material of the scintillation detector D3, or the construction materials of the detector head, reach

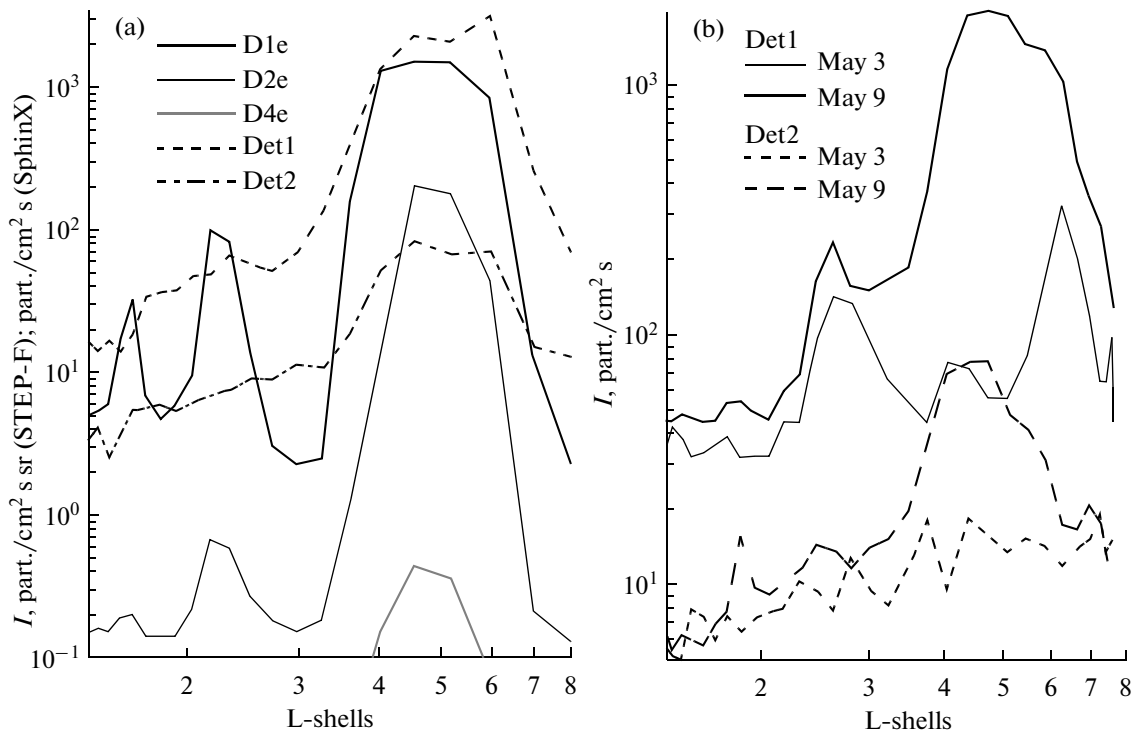


Fig. 6. The distribution of L-shells of particle fluxes in the RB in the Northern Hemisphere on the ninth (since the beginning of the day) ascending nodes of the spacecraft orbit in five recording channels of both devices on May 8, 2009 (a), and the distribution by L-shells of the particle fluxes in the RB in the Southern Hemisphere on the first descending node of the spacecraft orbit in the channels Det1 and Det2 on May 3 and 9.

at least the second layer of position-sensitive silicon matrix sensors. At the same time, the decrease of the value of E_{D4e} from ~ 335 keV for the BMA to ~ 240 keV for RBs also points to the softening of the energy spectrum in the RB, compared with the shape of the spectrum in the BMA.

Thus, knowing the values of E_{thr1} , E_{thr2} , and E_{D4e} , the nature of the energy spectrum of primary electrons can be assessed in a particular part of the Earth's magnetosphere. In turn, the shape and the slope of the spectrum may indicate a preferential recording of trapped, quasi-trapped, or precipitating electrons.

CONCLUSIONS

The joint analysis of data obtained by solar X-ray spectrometer SphinX and the electron and proton satellite telescope STEP-F, installed on the low-orbit satellite CORONAS-PHOTON, showed the dynamics of low-energy and ultra-relativistic electrons in the Brazilian Magnetic Anomaly and the outer radiation belt in the vicinity of the weak geomagnetic storm. Leading channels of energy spectrometers of the SphinX device contain information about the fluxes of low and medium energies. At the same time, in the records of the number of particles within the selected time periods, there is a contribution of both the direct electron

detection by active volumes of large area photodiodes, and the recording of secondary gamma quanta of different energies, caused by electron collisions with structural materials of the instrument, the TESIS observatory, and the spacecraft itself.

The effective threshold energies are determined for electron detection by the Det1 and Det2 sensors of the SphinX device and the D4e channel of the STEP-F telescope, which amounted to $E_{thr1} \approx 500$ keV, $E_{thr2} \approx 475$ keV, and $E_{D4e} \approx 335$ keV in the areas of the Brazilian Magnetic Anomaly with the relative values of the magnetic field of the Earth $B/B_0 \approx 1.2-1.6$. For the Earth's outer radiation belt, effective values for electron recording were, respectively, $E_{thr1} \approx 5$ keV, $E_{thr2} \approx 60$ keV, and $E_{D4e} \approx 240$ keV. These values are not strictly fixed. They are functions of the spatial position of the sensors in a particular area of charged radiation, whether in its center or at the periphery, as well as of the level of geomagnetic disturbance.

The experimental determination of displacements of ΔL values of L-shells in the outer radiation belt, on which peaks of distributions of particle fluxes were observed in the recording channels of both devices in the process of radial diffusion of electrons, relative to the initial allocation in the period before the storm, allowed us to determine the dependence of ΔL on the electron energy. Thus, the recording channels of the

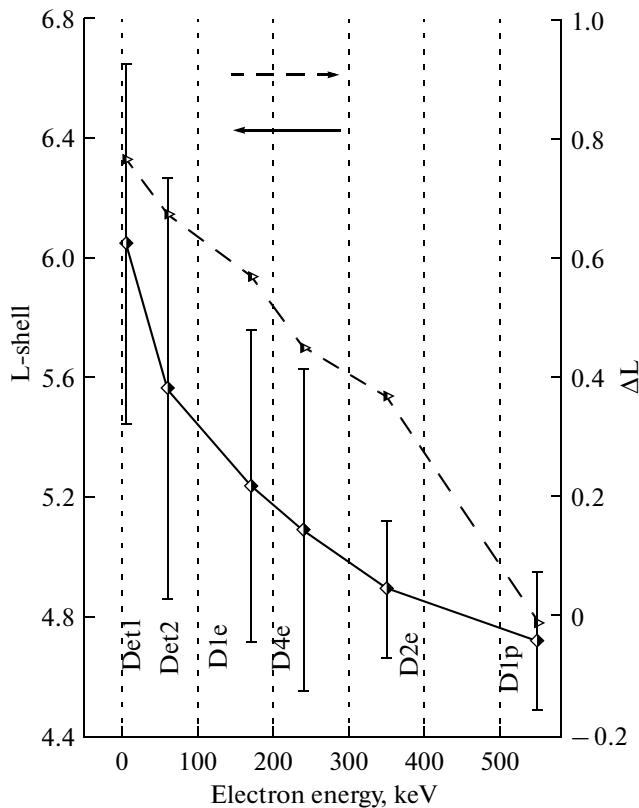


Fig. 7. The dependence of averaged values of L-shells for the period of May 1–14, 2009, with maximal fluxes of particles in the external RB (the left scale OY) on their energy for the ascending nodes of the ninth (since the beginning of the day) in the Northern Hemisphere (solid line). The dotted line shows the dependence on the electron energy of the largest displacements of maximal fluxes on the value of ΔL (the right scale of the axis OY) deep into the magnetosphere in the process of radial diffusion during the initial recovery phase of the magnetic storm on May 9–11 with respect to the initial positions prior to its beginning on May 2–3. Horizontal arrows show the graphs belonging to the left or right scale.

SphinX device supplemented and extended the energy range of recorded channels of the STEP-F device toward lower energies outside the Brazilian Magnetic Anomaly.

Finally, by the values of effective threshold recorded energies by both detectors of the SphinX spectrophotometer, it is possible to estimate the nature of the energy spectrum of primary electrons, and thus to indicate the preferential recording of trapped or precipitated electrons in a part of the Earth's magnetosphere. Given the low values of the effective threshold of recorded energies beyond the scope of the anomaly, as well as the narrow field of view, using the SphinX device it is possible to explore little-known

phenomena in the middle and low latitudes as connections with thunderstorm activity, reducing the resolution time of recording to the minimum possible.

ACKNOWLEDGMENTS

We thank the staff of the Institute of Astrophysics of the National Research Nuclear University “Moscow Engineering and Physics Institute” for systematic assistance in providing scientific and service data from the STEP-F device and the spacecraft as a whole.

This work was supported by the Program FP7/2007–2013 of the European Commission, project no. 218816 (The SOTERIA Project, www.soteria-space.eu), as well as by the Ministry of Education and Science of the Republic of Poland, project no. 203381736.

REFERENCES

- Arkhangelskaja, I.V., Amandjolova, D.B., Arkhangelsky, A.I., and Kotov, Yu.D., Features of Quasi-Stationary Precipitations according to the Data Obtained with the AVS-F Instrument Onboard the CORONAS-F Satellite, *Sol. Syst. Res.*, 2008, vol. 42, no. 6, pp. 536–542.
- Dudnik, A.V., Research of the Earth's Radiation Belts in May 2009 at Low-Orbit Satellite by Using STEP-F Satellite Telescope of Electrons and Protons, *Kosm. Nauka Tekhnol.*, 2010, vol. 16, no. 5, pp. 12–28.
- Dudnik, A.V., Persikov, V.K., Zalyubovsky, I.I., et al., High-Sensitivity STEP-F Spectrometer–Telescope for High-Energy Particles of the CORONAS-PHOTON Satellite Experiment, *Sol. Syst. Res.*, 2011, vol. 45, no. 3, pp. 212–220.
- Gburek, S., Siarkowski, M., Kepa, A., et al., Soft X-ray Variability over the Present Minimum of Solar Activity as Observed by SphinX, *Sol. Syst. Res.*, 2011a, vol. 45, no. 2, pp. 182–187.
- Gburek, S., Sylwester, J., Kowalinski, M., et al., SphinX Soft X-ray Spectrophotometer: Science Objectives, Design and Performance, *Sol. Syst. Res.*, 2011b, vol. 45, no. 3, pp. 189–199.
- Glyanenko, A.S., Kotov, Yu.D., Pavlov, A.V., et al., The AVS-F Experiment on Recording Rapidly Changing Fluxes of Cosmic and Gamma Radiation Prepared under the CORONAS-F Project, *Instrum. Experim. Tech.*, 2009, vol. 42, no. 5, pp. 596–603.
- Kotov, Yu.D., Scientific Goals and Observational Capabilities of the CORONAS-PHOTON Solar Satellite Project, *Sol. Syst. Res.*, 2011, vol. 45, no. 2, pp. 93–96.
- Kuznetsov, S.N., Myagkova, I.N., Yushkov, B.Yu., et al., Dynamics of the Earth Radiation Belts during Strong Magnetic Storms Based on CORONAS-F Data, *Sol. Syst. Res.*, 2007, vol. 41, no. 4, pp. 338–348.
- Sylwester, J., Kuzin, S., Kotov, Yu.D., et al., A Fast Solar Photometer in X-rays, *J. Astrophys. Astron.*, 2008, vol. 29, nos. 1–2, pp. 339–343.
- <http://www.amptek.com/xr100cr.html>